J. Plasma Physics (2013), vol. 79, part 5, pp. 629–633. © Cambridge University Press 2013
doi:10.1017/S0022377813000123

Dispersion relations of dust lattice waves in two-dimensional honeycomb configuration

B. FAROKHI

Department of physics, Faculty of science, Arak-University, 38156-8-8349 Arak, Iran
(b-farokhi@araku.ac.ir)

(Received 2 December 2012; revised 7 January 2013; accepted 14 January 2013; first published online 22 February 2013)

Abstract. The linear dust lattice waves propagating in a two-dimensional honeycomb configuration is investigated. The interaction between particles is considered up to distance $2a$, i.e. the third-neighbor interactions. Longitudinal and transverse (in-plane) dispersion relations are derived for waves in arbitrary directions. The study of dispersion relations with more neighbor interactions shows that in some cases the results change physically. Also, the dispersion relation in the different direction displays anisotropy of the group velocity in the lattice. The results are compared with dispersion relations of the waves in the hexagonal lattice.

1. Introduction

Dusty plasma crystalline is a formation of strongly coupled dust grains, due to the high electric charge acquired by massive dust particles, high densities and low temperatures encountered in such plasmas. Crystal formation and dynamics have been studied in various discharge experiments and simulations (Thomas et al. 1994a; Melandso 1996; Hamaguchi et al. 1997; Nunomura et al. 2000; Misawa et al. 2001; Vaulina et al. 2002; Farokhi et al. 2006b; Bonitz et al. 2010). The simplest model for the waves in plasma crystals is the one-dimensional (1D) linear approximation of dust chain (Chu and Lin 1994; Pieper et al. 1996; Vladimirov et al. 1997). The force equilibrium in the dust crystal is ensured by the sheath electric force that balances gravity at the levitation height. Hence, in experiments complex plasmas often form either a monolayer or a cloud with a few layers, i.e. 2D or quasi-2D systems. Most Coulomb crystal structures that have been reported to be observed in dusty plasmas have 2D hexagonal (Wang et al. 2001; Kourakis and Shukla 2004; Farokhi et al. 2006a).

The honeycomb lattices have been studied in various experiments and simulations (Srikantha et al. 2006; Kamimura et al. 2007; Peleg et al. 2007; Tang et al. 2007; Law et al. 2008; Koukouloyannis et al. 2010), but in dusty plasma lattices, it is a new feature of research. For the first time, Srikantha et al. (2006) predicted the honeycomb lattice in dusty plasma crystals. Then, Kamimura et al. (2007) studied the structures of Coulomb clusters by numerical simulation. They showed that the dust crystal can be formed in a honeycomb configuration (Kamimura et al. 2007). A little investigation has been done on the honeycomb dusty plasma lattice, which it is not enough for the diagnosis of dust-lattice crystals (Law et al. 2008; Koukouloyannis et al. 2010).

In this paper, we consider the linear longitudinal and transverse oscillations (which may propagate in-plane and in any direction) in a honeycomb 2D monolayer. We calculate the force on the particles up to the third-neighbor interactions.

2. Basic equations

Consider a 2D honeycomb crystal with lattice spacing a consisting of negative charge dust grains Q and mass M, modeled as point charges. We may expand the Debye–Hückel (DH) interaction potential energy, namely $U(r) = Q^2 \exp(-r/\lambda_D)/4\pi\varepsilon_0 r$ around equilibrium ($r = r_0$). The DH potential is a good approximation for all cases without streaming electrons or ions. In the presence of the ion flow, the DH potential is shown to be valid only in the direction perpendicular to the ion speed, i.e. the DH potential is valid in the x-y plane. The pair interaction can be represented by the DH potential with a shielded length $\lambda_D \sim \lambda_{De}$ that is close to the electron Debye length (Thomas et al. 1994b). We expand the DH potential and keep until the linear term in force,

$$U(r) \cong \frac{1}{2} G (r - r_0)^2, \tag{1.1}$$

where

$$G = \left(\frac{\partial^2 U}{\partial r^2}\right)\Big|_{r=r_0} = G_0 \frac{2 + 2(\kappa\tilde{r}) + (\kappa\tilde{r})^2}{(\kappa\tilde{r})^3} \exp(-\kappa\tilde{r}), \tag{1.2}$$

$$G_0 = Q^2/4\pi\varepsilon_0\lambda_D^3, \quad \tilde{r} = r_0/a.$$

The lattice parameter $\kappa = a/\lambda_D$ is a positive real number, practically taking values of $\kappa \cong 1$–1.5 in real discharge experiments (Thomas et al. 1994a). We term the spring constant $G_i (i = 1, 2, 3)$ for $\tilde{r} = 1, \sqrt{3}, 2$, respectively. Dust particles are assumed to be elastically bound to the center of the system, and a force acting on dust particles increases linearly with their displacement δr. The parabolic confinement potential in the $x - y$ plane is smooth in comparison with the spring constant of the

https://doi.org/10.1017/S0022377813000123 Published online by Cambridge University Press

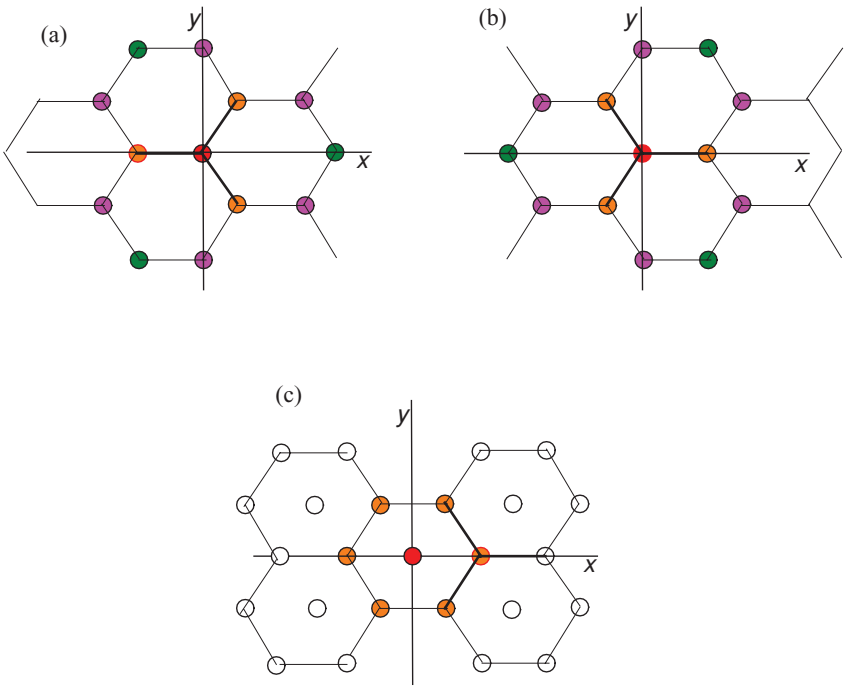


Figure 1. (Colour online) Two-dimensional dust lattice (a) honeycomb type 1 (b) honeycomb type 2 (c) hexagonal.

interaction potential, i.e. $M\Omega_x^2 \cong M\Omega_y^2 \ll G_1$:

$$U_{\text{con}} = \frac{1}{2}M\Omega_x^2 x^2 + \frac{1}{2}M\Omega_y^2 y^2. \tag{1.3}$$

Experimentally a confining potential can be controlled by shaping a plasma through adjustment of the configuration of electrodes. The potential has a 2D symmetric configuration, i.e. $\Omega_x \cong \Omega_y = \Omega$.

Figure 1 shows that the honeycomb configuration has three nearest neighbors ($r_0 = a$), six particles as second neighbors ($r_0 = a\sqrt{3}$), and three particles as third neighbors ($r_0 = 2a$). Figure 3 shows the spring constant for more neighbor interactions. Let the (n,m)th particle location define the origin, then there are two configurations for the first neighbors which they defined as type 1 and type 2 in Fig. 1. The positions of the first neighbors for type 1 are $(-a/2, \pm\sqrt{3}a/2)$, $(a, 0)$ and for type 2 are $(a/2, \pm\sqrt{3}a/2)$, $(-a, 0)$.

Figure 2 shows the potential energy of the (n,m)th particle as a function of the dust grain deviation δr from equilibrium. The potential energy and the force exerted on the (n,m)th particle are different for type 1 and type 2, so up to the first-neighbor interaction (FNI), the result is not correct and we should calculate more neighbor interactions for the honeycomb lattice. In the special case, when the particles deviate in the $\phi = \pi/6$ and $\phi = \pi/2$ directions (the angle ϕ representing the angle between the direction of the particle's deviation δr and the x axis), the curve of the potential energy for type 1 and type 2 is the same, and the calculation up to FNI is allowable. The slope of the potential curves shows that the hexagonal lattice is more stable than the honeycomb lattice. In the hexagonal lattice, the particles

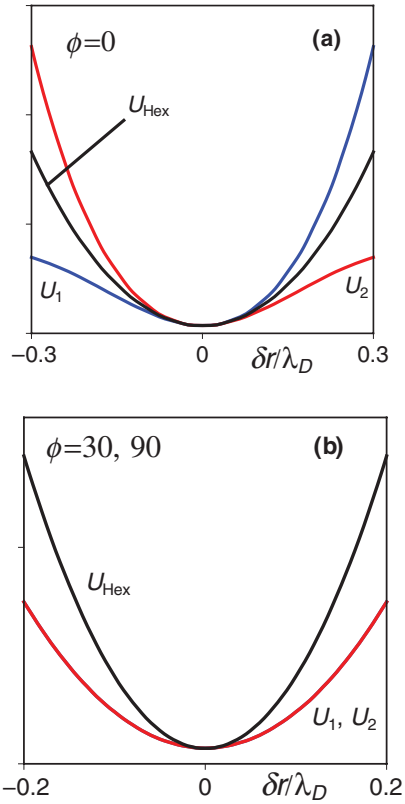


Figure 2. (Colour online) The normalized potential energy as a function of dust grain deviation $\delta r/\lambda_D$ for (a) $\phi = 0$ (particles deviate in the x direction), (b) $\phi = \pi/6$ and $\phi = \pi/2$.

are closer than the honeycomb and so the minimum of energy is deeper, but in Fig. 2, we have normalized the potential energy (with the same minimum) for all curves. Due to symmetry structure of the hexagonal lattice, the

https://doi.org/10.1017/S0022377813000123 Published online by Cambridge University Press

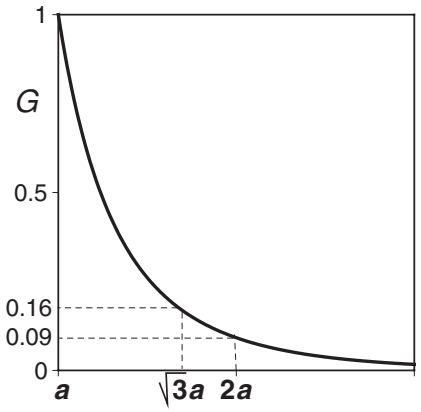


Figure 3. The dimensionless characteristic coefficient G/G_1 as a function of the normalized distance between particles for $\kappa = 1$.

calculation up to the FNI is correct, approximately. Both potentials in the honeycomb and hexagonal lattices have a minimum at equilibrium, i.e. for in-plane vibration, the first derivative of the neighbor interactions at equilibrium is zero.

However, if the particles in the type 1 configuration are not at their equilibrium positions, we then define 12 lengths r_i, $i = 1, \ldots, 12$ to represent the distances from the particle (n, m) to neighbors, respectively,

$$r_i = \sqrt{(a_{ix} + \Delta u_i)^2 + (a_{iy} + \Delta v_i)^2}, \tag{1.4}$$

$$a_{ix} = a(1, -1/2, -1/2, 3/2, 3/2, -3/2, -3/2, 0, 0, 1, 1, -2), \tag{1.5}$$

$$a_{iy} = a(0, \sqrt{3}/2, -\sqrt{3}/2, \sqrt{3}/2, -\sqrt{3}/2, \sqrt{3}/2, -\sqrt{3}/2, \sqrt{3}, -\sqrt{3}, \sqrt{3}, -\sqrt{3}, 0). \tag{1.6}$$

For the type 2 configuration, we define 12 new lengths to represent the distances from the particle (n, m) to neighbors, respectively,

$$r_i' = \sqrt{(a_{ix} + \Delta u_i)^2 + (a_{iy} + \Delta v_i)^2}, \tag{1.7}$$

$$a_{ix} = a(-1, 1/2, 1/2, 3/2, 3/2, -3/2, -3/2, 0, 0, -1, -1, 2), \tag{1.8}$$

$$a_{iy} = a(0, \sqrt{3}/2, -\sqrt{3}/2, \sqrt{3}/2, -\sqrt{3}/2, \sqrt{3}/2, -\sqrt{3}/2, \sqrt{3}, -\sqrt{3}, \sqrt{3}, -\sqrt{3}, 0), \tag{1.9}$$

where u_i, v_i (for $i = 1, \ldots, 12$) denote the displacements of the particles from their equilibrium positions in the x, y, z directions, respectively, and $\Delta u_i = u_i - u_{nml}$, $\Delta v_i = v_i - v_{nml}$. The force exerted on the particle (n, m) is given by

$$F_x = G_1 \sum_{i=1}^{3} (r_i - a) \frac{a_{ix} + \Delta u_i}{r_i} + G_2 \sum_{i=4}^{9} (r_i - a\sqrt{3}) \times \frac{a_{ix} + \Delta u_i}{r_i} + G_3 \sum_{i=10}^{12} (r_i - 2a) \frac{a_{ix} + \Delta u_i}{r_i}, \tag{1.10}$$

$$F_y = G_1 \sum_{i=1}^{3} (r_i - a) \frac{a_{iy} + \Delta v_i}{r_i} + G_2 \sum_{i=4}^{9} (r_i - a\sqrt{3}) \times \frac{a_{iy} + \Delta v_i}{r_i} + G_3 \sum_{i=10}^{12} (r_i - 2a) \frac{a_{iy} + \Delta v_i}{r_i}. \tag{1.11}$$

For in-plane small amplitude waves, we may neglect the nonlinear terms and obtain the equation of motions:

$$\begin{aligned} M \frac{d^2 u_{nm}}{dt^2} = {} & -M\Omega^2 u_{nm} + G_1[4u_{n+1,m} + (u_{n-1/2,m+\sqrt{3}/2} \\ & + u_{n-1/2,m-\sqrt{3}/2}) - 6u_{n,m} - \sqrt{3}(v_{n-1/2,m+\sqrt{3}/2} \\ & - v_{n-1/2,m-\sqrt{3}/2})]/4 + G_2[3(u_{n+3/2,m+\sqrt{3}/2} + u_{n+3/2,m-\sqrt{3}/2} \\ & + u_{n-3/2,m+\sqrt{3}/2} + u_{n-3/2,m-\sqrt{3}/2} - 4u_{n,m}) \\ & + \sqrt{3}(v_{n+3/2,m+\sqrt{3}/2} - v_{n+3/2,m-\sqrt{3}/2} - v_{n-3/2,m+\sqrt{3}/2} \\ & + v_{n-3/2,m-\sqrt{3}/2})]/4 + G_3[(u_{n+1,m+\sqrt{3}} + u_{n+1,m-\sqrt{3}})/4 \\ & + u_{n-2,m} - 3u_{n,m}/2 + \sqrt{3}(v_{n+1,m+\sqrt{3}} - v_{n+1,m-\sqrt{3}})/4], \end{aligned} \tag{1.12}$$

$$\begin{aligned} M \frac{d^2 v_{nm}}{dt^2} = {} & -M\Omega^2 v_{nm} + G_1[\sqrt{3}(-u_{n-1/2,m+\sqrt{3}/2} \\ & + u_{n-1/2,m-\sqrt{3}/2})/4 + 3(v_{n-1,m+\sqrt{3}/2} + v_{n-1,m-\sqrt{3}/2} \\ & - 2v_{nm})/4] + G_2[\sqrt{3}(u_{n+3/2,m+\sqrt{3}/2} - u_{n+3/2,m-\sqrt{3}/2} \\ & - u_{n-3/2,m+\sqrt{3}/2} + u_{n-3/2,m-\sqrt{3}/2})/4 + (v_{n+3/2,m+\sqrt{3}/2} \\ & + v_{n+3/2,m-\sqrt{3}/2} + v_{n-3/2,m+\sqrt{3}/2} + v_{n-3/2,m-\sqrt{3}/2} \\ & - 4v_{n,m})/4 + (v_{n,m+\sqrt{3}} + v_{n,m-\sqrt{3}} - 2v_{nm})] \\ & + G_3[\sqrt{3}(u_{n+1,m+\sqrt{3}} - u_{n+1,m-\sqrt{3}})/4 + 3(v_{n+1,m+\sqrt{3}} \\ & + v_{n+1,m-\sqrt{3}} - 2v_{nm})/4]. \end{aligned} \tag{1.13}$$

3. The linear modes

Waves can propagate along an arbitrary direction, which is denoted by angle θ, representing the angle between the wavevector k and a primitive translation vector (along the x axis), i.e. $k_x = k\cos\theta$ and $k_y = k\sin\theta$. Considering phonons of the type,

$$u_{n,m} = u_o \exp(-i\omega t) \exp[ika(n\cos\theta + m\sin\theta)], \tag{2.1}$$

$$v_{n,m} = v_o \exp(-i\omega t) \exp[ika(n\cos\theta + m\sin\theta)]. \tag{2.2}$$

By letting (2.1)–(2.2) into (1.12)–(1.13) and neglecting nonlinear terms, we thus obtain the system of equations

$$\left[\omega^2 + A_1\right] u_{nm} + A_2 v_{nm} = 0, \tag{2.3}$$

$$A_3 u_{nm} + \left[\omega^2 + A_4\right] v_{nm} = 0, \tag{2.4}$$

https://doi.org/10.1017/S0022377813000123 Published online by Cambridge University Press

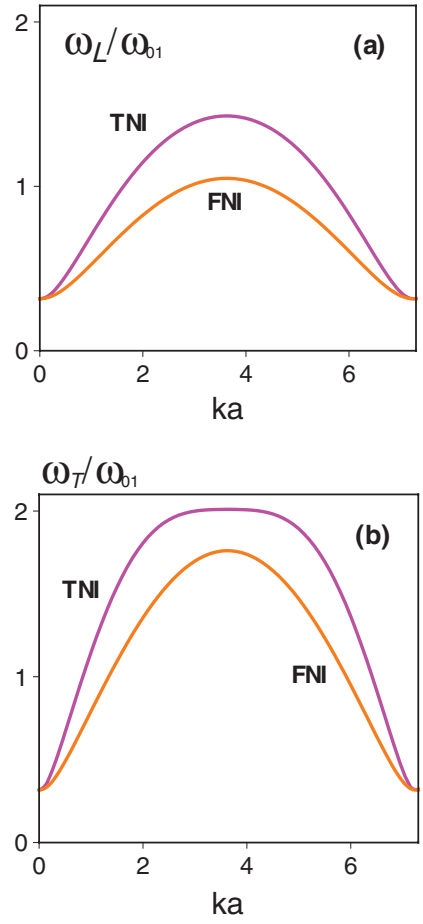


Figure 4. (Colour online) Dispersion relations of the waves in the honeycomb lattice which it propagates in the y direction. (a) The longitudinal and (b) the transverse lattice modes, up to the FNI (orange line) and up to the third-neighbor interaction (TNI, pink line).

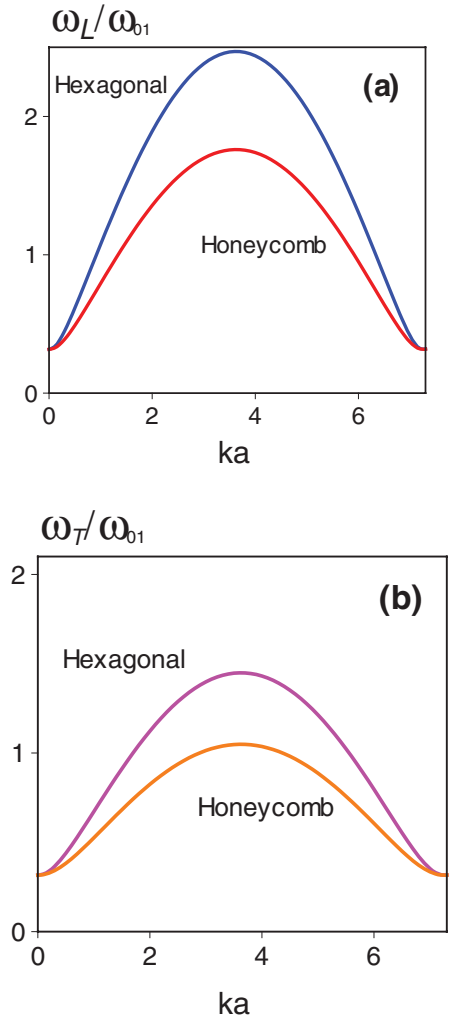


Figure 5. (Colour online) Comparison of the dispersion relation between the honeycomb and the hexagonal lattices up to the FNI (a) the longitudinal wave and (b) the transverse wave.

where

$$A_1 = -\Omega^2 + \omega_{01}^2\{\exp(ika\cos\theta) + \exp(-ika\cos\theta/2) \times \cos(ka\sqrt{3}\sin\theta/2)/2 - 3/2\} + 3\omega_{02}^2 \times [\cos(\sqrt{3}ka\sin\theta/2)\cos(3ka\cos\theta/2) - 1] + \omega_{03}^2[0.5\exp(ika\cos\theta)\cos(\sqrt{3}ka\sin\theta) + \exp(-2ika\cos\theta) - 1.5],$$

$$A_2 = -i\sqrt{3}\omega_{01}^2\exp(-ika\cos\theta/2)\sin(\sqrt{3}ka\sin\theta/2)/2 - \sqrt{3}\omega_{02}^2\sin(3ka\cos\theta/2) \times \sin(\sqrt{3}ka\sin\theta/2) + i\sqrt{3}\omega_{03}^2\exp(ika\cos\theta)\sin(\sqrt{3}ka\sin\theta)/2,$$

$$A_3 = -i\sqrt{3}\omega_{01}^2\exp(-ika\cos\theta/2)\sin(\sqrt{3}ka\sin\theta/2)/2 - \sqrt{3}\omega_{02}^2\sin(3ka\cos\theta/2)\sin(\sqrt{3}ka\sin\theta/2) + i\sqrt{3}\omega_{03}^2\exp(ika\cos\theta)\sin(\sqrt{3}ka\sin\theta)/2,$$

$$A_4 = -\Omega^2 + 3\omega_{01}^2[\exp(-ika\cos\theta)\cos(\sqrt{3}ka\sin\theta/2) - 1]/2 + \omega_{02}^2[\cos(\sqrt{3}ka\sin\theta/2)\cos(3ka\cos\theta/2) + 2\cos(\sqrt{3}ka\sin\theta) - 3] + 3\omega_{03}^2[\exp(ika\cos\theta) \times \cos(\sqrt{3}ka\sin\theta) - 1]/2,$$

where $\omega_{0i}^2 = G_i/M$. We obtain the dispersion relation by setting the determinant of the coefficients equal to zero,

$$\omega^2 = \frac{1}{2}[-(A_1 + A_4) \pm \sqrt{(A_1 - A_4)^2 + 4A_2A_3}]. \quad (2.5)$$

By letting $r_i' \to r_i$, we will obtain the dispersion relaton of lattice type 2. In the special case $\theta = \pi/2$ (for wave propagating in the y directon),

$$A_1 = -\Omega^2 - (\omega_{01}^2 + 6\omega_{02}^2)\sin^2(ka\sqrt{3}/4) - \omega_{03}^2\sin^2(ka\sqrt{3}/2),$$

$$A_2 = A_3 = -i\sqrt{3}[\omega_{01}^2\sin(\sqrt{3}ka/2) - \omega_{03}^2\sin(\sqrt{3}ka)]/2,$$

https://doi.org/10.1017/S0022377813000123 Published online by Cambridge University Press

$$A_4 = -\Omega^2 - \left(3\omega_{01}^2 + 2\omega_{02}^2\right)\sin^2(\sqrt{3}ka/4)$$
$$-4\omega_{02}^2\sin^2(\sqrt{3}ka/2) - 3\omega_{03}^2\sin^2(\sqrt{3}ka/2).$$

Figures 4(a) and (b) show the normalized longitudinal and transverse dispersion relations of the wave propagating in the special case $\theta = \pi/2$, for the honeycomb lattice (type 1 and type 2). The study of dispersion relations with more neighbor interactions shows that in some cases the results change physically.

Figures 5(a) and (b) compare longitudinal and transverse waves of the honeycomb and hexagonal lattice up to the FNI. Both waves propagate in the y direction. The group velocity of the wave in the hexagonal lattice is more than the honeycomb lattice. The different group velocity is due to the different particle spacing and so due to the different slope of the potential energy curve.

4. Conclusions

In summary, the longitudinal and the transverse (in-plane) of the linear dust-lattice waves are found in the honeycomb lattice. The force exerted on the dust particles in the 2D honeycomb dust lattice is found and compared with the hexagonal one. The symmetry structure of the hexagonal lattice allows us to find the dispersion relations up to the FNI for simplicity, but in the honeycomb lattice just for the special case the symmetry occurs. In general, we should calculate up to the more neighbor interaction.

A comparison of the longitudinal and the transverse dispersion relations between the honeycomb and the hexagonal lattices (Farokhi et al. 2006a) shows that the group velocity of the waves in the hexagonal lattice is more than the group velocity in the honeycomb lattice.

References

Bonitz, M., Henning, C. and Block, D. 2010 *Rep. Prog. Phys.* **73**, 066501. doi:10.1083/0034-4885/73/6/066501

Chu, J. H. and Lin, I. 1994 *Phys. Rev. Lett.* **72**, 4009. doi:10.1103/PhysRevLett.72.4009

Farokhi, B., Kourakis, I. and Shukla, P. K. 2006a *Physics Lett.* A **355**, 122. doi:10.1016/j.Physleta.2006.02.016

Farokhi, B., Kourakis, I. and Shukla, P. K. 2006b *Phys. Plasmas* **13**, 122304. doi:10.1063/1.2400594

Hamaguchi, S., Farouki, R. T. and Dubin, D. H. E. 1997 *Phys. Rev.* E **56**, 4671. doi:10.1103/PhysRevE.56.4671

Kamimura, T., Suga, Y. and Ishihara, O. 2007 *Phys. Plasmas* **14**, 123706.

Koukouloyannis, V., Kevrekidis, P. G., Law, K. J. H., Kourakis, I. and Frantzeskakis, D. J. 2010 *J. Phys.* A*: Math. Theor.* **43**, 235101.

Kourakis, I. and Shukla, P. K. 2004 *Phys. Plasmas* **11**, 1384. doi:10.1063/1.1687417

Law, K. J. H., Kevrekidis, P. G., Koukouloyannis, V., Kourakis, I., Frantzeskakis, D. J. and Bishop, A. R. 2008 *Phys. Rev.* E **78**, 066610.

Melandso, F. 1996 *Phys. Plasmas* **3**, 3890. doi:10.1063/1.871577

Misawa, T., Ohno, N., Asano, K., Sawai, M., Takamura, S. and Kaw, P. K. 2001 *Phys. Rev. Lett.* **86**, 1219. doi:10.1103/PhysRevLett.86.1219

Nunomura, S., Samsonov, D. and Goree, J. 2000 *Phys. Rev. Lett.* **84**, 5141. doi:10.1103/PhysRevLett.84.5141

Peleg, O., Bartal, G., Freedman, B., Manela, O., Segev, M. and Christodoulides, D. 2007 *Phys. Rev. Lett.* **98**, 103901.

Pieper, J. B., Goree, J. and Quinn, R. A. 1996 *J. Vac. Sci. Technol.* A **14**, 519. doi:10.1116/1.580118

Srikantha, P. A., Woodhouse, J. and Fleck, N. A. 2006 *J. Acoust. Soc. Am.* **119**, 1995.

Tang, Z., Zhang, H., Ye, Y., Zhao, C., Peng, R., Wen, S. and Fan, D. 2007 *Solid State Commun.* **141**, 183.

Thomas, H., Morfill, G. E., Demmel, V., Goree, J., Feuerbacher, B. and Mohlmann, D. 1994a *Phys. Rev. Lett.* **73** 652. doi:10.1103/PhysRevLett.73.652

Thomas, H., Morfill, G. E., Demmel, V., Goree, J., Feuerbacher, B. and Mohlmann, D. 1994b *Phys. Rev. Lett.* **73**, 652.

Vaulina, O., Khrapak, S. and Morfill, G. E. 2002 *Phys. Rev.* E **66**, 016404. doi:10.1103/PhysRevE.66.016404

Vladimirov, S. V., Shevchenko, P. V. and Cramer, N. F. 1997 *Phys. Rev.* E **56**, R74. doi:10.1103/PhysRevE.56.R74

Wang, X., Bhattacharjee, A. and Hu, S. 2001 *Phys. Rev. Lett.* **86**, 2569. doi:10.1103/PhysRevLett.86.2569

https://doi.org/10.1017/S0022377813000123 Published online by Cambridge University Press